PAPER • OPEN ACCESS

Dynamical formation of a magnetic polaron in a two-dimensional quantum antiferromagnet

To cite this article: A Bohrdt *et al* 2020 *New J. Phys.* **22** 123023

New Journal of Physics
The open access journal at the forefront of physics

Deutsche Physikalische Gesellschaft DPG
IOP Institute of Physics

Published in partnership with: Deutsche Physikalische Gesellschaft and the Institute of Physics

OPEN ACCESS

RECEIVED
17 August 2020

REVISED
15 November 2020

ACCEPTED FOR PUBLICATION
2 December 2020

PUBLISHED
21 December 2020

PAPER

Dynamical formation of a magnetic polaron in a two-dimensional quantum antiferromagnet

A Bohrdt[1,2,*], F Grusdt[1,2] and M Knap[1,2]

[1] Department of Physics and Institute for Advanced Study, Technical University of Munich, 85748 Garching, Germany
[2] Munich Center for Quantum Science and Technology (MCQST), Schellingstr. 4, D-80799 München, Germany
[*] Author to whom any correspondence should be addressed.

E-mail: annabelle.bohrdt@tum.de

Keywords: magnetic polaron formation, multi-stage dynamics, Fermi–Hubbard, parton theory, pattern recognition, time-dependent DMRG

Supplementary material for this article is available online

Abstract

Tremendous recent progress in the quantum simulation of the Hubbard model paves the way to controllably study doped antiferromagnetic Mott insulators. Motivated by these experimental advancements, we numerically study the real-time dynamics of a single hole created in an antiferromagnet on a square lattice, as described by the t–J model. Initially, the hole spreads ballistically with a velocity proportional to the hopping matrix element. At intermediate to long times, the dimensionality as well as the spin background determine the hole dynamics. A hole created in the ground state of a two dimensional (2D) quantum antiferromagnet propagates again ballistically at long times but with a velocity proportional to the spin exchange coupling, showing the formation of a magnetic polaron. We provide an intuitive explanation of this dynamics in terms of a parton construction, which leads to a good quantitative agreement with the numerical tensor network state simulations. In the limit of infinite temperature and no spin exchange couplings, the dynamics can be approximated by a quantum random walk on a Bethe lattice with coordination number $\tilde{z} = 4$. Adding Ising interactions corresponds to an effective disordered potential, which can dramatically slow down the hole propagation, consistent with subdiffusive dynamics. The study of the hole dynamics paves the way for understanding the microscopic constituents of this strongly correlated quantum state.

Understanding the properties of a single mobile hole doped into an antiferromagnet allows one to reveal the interplay of spin and charge degrees of freedom. This constitutes a crucial step in the theoretical description of the Fermi–Hubbard model and by extension, strongly correlated cuprate compounds [1, 2].

In the limit of strong interactions, the Fermi–Hubbard model can be approximated by the t–J model. In two dimensions and for a single hole, the latter is described by the Hamiltonian [3],

$$\hat{\mathcal{H}}_{t-J} = -t\sum_{\langle\vec{i},\vec{j}\rangle,\sigma}\mathcal{P}\left(\hat{c}^{\dagger}_{\vec{i},\sigma}\hat{c}_{\vec{j},\sigma} + \text{h.c.}\right)\mathcal{P} + J\sum_{\langle\vec{i},\vec{j}\rangle}\hat{\mathbf{S}}_{\vec{i}}\cdot\hat{\mathbf{S}}_{\vec{j}}, \tag{1}$$

where $\mathcal{P}$ projects on states with less than two fermions per site. The first term describes tunneling of holes with amplitude t and the second term denotes spin–exchange interactions with coupling constant $J = 4t^2/U$, where U is the bare interaction. In the absence of doping, the ground state of the two dimensional system is effectively a Heisenberg antiferromagnet with long-range spin correlations.

Here we study the dynamics of the system after the creation of one hole at the origin, which can move through the antiferromagnet according to the tunneling matrix element t. The motion of the hole distorts the surrounding spin order and leads to an interplay of spin and charge dynamics. Even though this problem is most intuitively described in real space, a predominant part of research has focused on frequency and momentum space properties, which are most directly accessible in solid-state experiments.

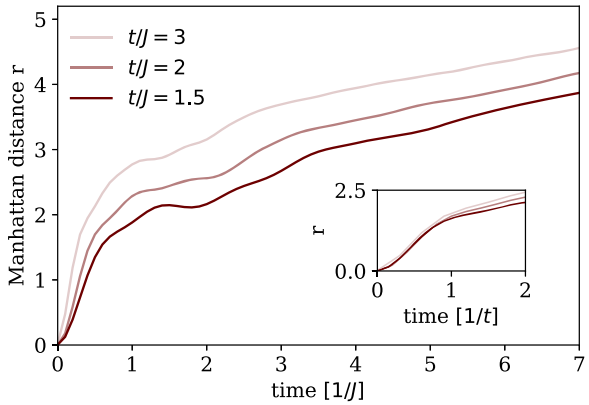

Figure 1. Dynamics of a hole in the two-dimensional t–J model on a square lattice for $t/J = 1.5, 2, 3$ with cylinder length $L_x = 18$ and circumference $L_y = 4$. The plot shows the average Manhattan distance to the origin as a function of time. The initial spreading with velocity proportional to the hole hopping t coincides for all values of the hopping for times in units of $1/t$ (inset). For longer times, the Manhattan distance increases with a slower rate determined by the spin exchange J and is independent of the hopping t.

An important example is the spectral function [4–8], which can be expressed as an overlap of the initial state with the time-evolved state with a single hole. Notable exceptions are the works in reference [9], where the phase of the hole hopping is quenched, reference [10], where the dynamics of a pinned hole in a one dimensional system with a staggered magnetic field is studied, and references [11–16].

Creating a hole in an antiferromagnetic background realizes a local high energy excitation that is best probed with local resolution. The tremendous progress in quantum gas microscopy in recent years [17–26] has sparked an increasing interest in real space properties and the analysis of single snapshots obtained in projective measurements. In particular, related experiments in one dimension (1D) have recently demonstrated spin–charge separation in space and time [27].

Here we use a matrix-product-operator based time evolution [28, 29, 43] on a cylinder with four legs [30, 44] to efficiently calculate the dynamics of a hole introduced into a spin system according to the t–J Hamiltonian (1). We find that the hole spreads differently at short and long times, see figure 1, where the Manhattan distance

$$r = \sum_x \sum_y (|x| + |y|) \cdot n^h(x, y) \tag{2}$$

is shown. Here, $n^h(x, y) = \langle 1 - \sum_\sigma \hat{c}^\dagger_{(x,y),\sigma} \hat{c}_{(x,y),\sigma} \rangle$ is the hole density at site (x, y) and the hole is created in the origin. At short times, the hole propagates ballistically with a velocity proportional to t, see inset of figure 1. However, at a time $1/J$, the propagation slows down. We explain our numerical findings by a parton construction, where the excitation created in the system is decomposed into a spinon, carrying the spin quantum number, and a chargon, carrying the charge [31–34]. The propagation of the hole at intermediate and long times is therefore dominated by the slow spinon dynamics. The ballistic spreading with a velocity proportional to the spin exchange J at long times is due to the finite quasiparticle weight of the magnetic polaron.

1. Dimensional crossover from 1D to 2D

The constituents used to describe excitations in the t–J model carry either spin (spinons) or charge (chargon). In one spatial dimension spin–charge separation occurs; spinon and chargon are deconfined and propagate with different velocities [27, 35].

In one dimension, the independent dynamics of the quasiparticles can be understood in squeezed space, where sites occupied by a hole are removed from the lattice, such that the system is described by the combined information of hole positions and spin configuration [22, 36]. Most importantly, the motion of a hole cannot change the relative positions of the spins in one dimension. A hole created in the ground (or low temperature) state of the one-dimensional system always spreads ballistically with a velocity proportional to the hopping amplitude t, as recently shown in a quantum gas microscope [27].

In a cold atom experiment realizing the Fermi–Hubbard model, the crossover from one to two dimensions can be studied by tuning the lattice depth in one spatial direction [25]. In particular, the interaction U stays constant while the ratio between the hopping in y-direction t_y and the hopping in x-direction t_x, t_y/t_x, is tuned, and upon mapping the Fermi–Hubbard model to the t–J model, the spin

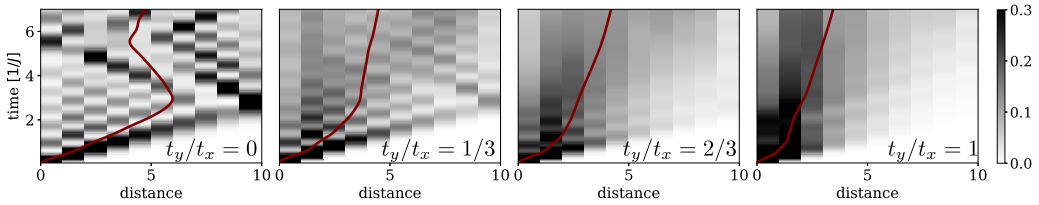

Figure 2. Dimensional crossover from 1D to 2D. Distance of the hole to the origin along the cylinder for $t_y/t_x = 0, 1/3, 2/3, 1$ for a cylinder of length $L_x = 19$ sites with $t_x/J_x = 2$. The quantity shown is the hole density, summed along y-direction over the four legs of the cylinder, as a function of distance in x-direction and time. In the one-dimensional case, $t_y/t_x = 0$, the hole dynamics are coherent and the hole spreads ballistically until it reaches the edge of the cylinder. Remnants of this behavior are still visible for $t_y/t_x = 1/3$ for the system sizes considered here and the same boundary effects as in one dimension appear. For $t_y/t_x = 2/3$ the velocity of the hole propagation is significantly reduced after the initial fast dynamics. Red lines show the mean value of the distance to the origin along the cylinder.

exchange couplings become $J_y/J_x = t_y^2/t_x^2$. Here, $J_{x(y)}$ are the Heisenberg-type spin exchange couplings in $x(y)$-direction of the lattice.

In figure 2 the dynamics of the hole is studied for different values of t_y/t_x at a fixed value of $t_x/J_x = 2$. For $t_y/t_x = 0$, we observe coherent hole dynamics as expected from spin–charge separation. For finite transverse couplings $t_y/t_x > 0$, the one-dimensional picture of spin–charge separation breaks down. While at short times, the spreading of the hole along the finite size cylinder still resembles the coherent dynamics of $t_y/t_x = 0$, at longer times, the mean distance to the origin increases significantly slower in the case of finite t_y/t_x (red lines).

The qualitative change in the hole dynamics can be understood from a parton construction of spinons and chargons [34]. Once the hopping in the second dimension is turned on, the hole motion distorts the spin background and frustrates the antiferromagnetic correlations of the system. This energy cost increases as the chargon hops away from the spinon and the chargon motion is therefore associated with a potential energy cost for the spin system. The competition between kinetic energy of the hole and potential energy of the spin system leads to an emergent length scale, which can be observed in figure 2 as the distance at which the velocity of the propagation changes; see [37] for more details.

2. Chargon and spinon dynamics in 2D

For $t_y = t_x = t$, we observe a separation of time scales in the hole dynamics, see figure 1. The hole shows fast ballistic spreading initially until a time $\approx 1/t$, at which its velocity is drastically reduced. At longer times $\approx 1/J$, the distance of the hole to the origin continues to increase linearly but at a slower rate. Our analysis for different values of t/J in figure 1 demonstrates that the initial dynamics are universal and do not depend on the value of J. At long times we observe slow spreading with a velocity essentially independent of t.

Within the geometric string theory (GST) [33, 34], this behavior can be understood as follows. The motion of the chargon displaces the spins, leading to an increase of energy by the string tension per bond. For a straight string, the string tension is given by

$$\frac{\mathrm{d}E_{\mathrm{pot}}}{\mathrm{d}l} = 2J \cdot \left(C_{\mathbf{e}_x+\mathbf{e}_y} - C_{\mathbf{e}_x}\right), \tag{3}$$

because spins which were diagonal next nearest neighbors before become nearest neighbors. Here, $C_{\mathrm{d}} = \langle\psi_0|\, \hat{\mathbf{S}}_{\mathbf{d}} \cdot \hat{\mathbf{S}}_{\mathbf{0}}\, |\psi_0\rangle$ and $|\psi_0\rangle$ is the initial state before the creation of the hole, see [37]. The chargon is therefore bound to the spinon by a string of displaced strings, where the length of this string is determined by the string tension [34].

Assuming a frozen spin background, the backaction onto the spin states is neglected and the chargon moves in a frame relative to the spinon. Up to self-retracing parts, all paths of the chargon are assumed to be distinguishable since they lead to different spin configurations in almost all cases. The chargon therefore effectively moves on a Bethe lattice, the origin of which corresponds to the position of the spinon. Each site on the Bethe lattice is associated with a potential energy, which increases approximately linear with the depth in the Bethe lattice and thus effectively limits the spread of the chargon. The GST comparison shown in figure 3 is based on the exact potential given by the different possible paths. We also call this non-linear string theory as opposed to the linear string theory, where the potential is approximated as linear [37]. Note that this theoretical approach is not limited to the ground state of the t–J model, but can be applied generally as long as the system has significant short-range antiferromagnetic order.

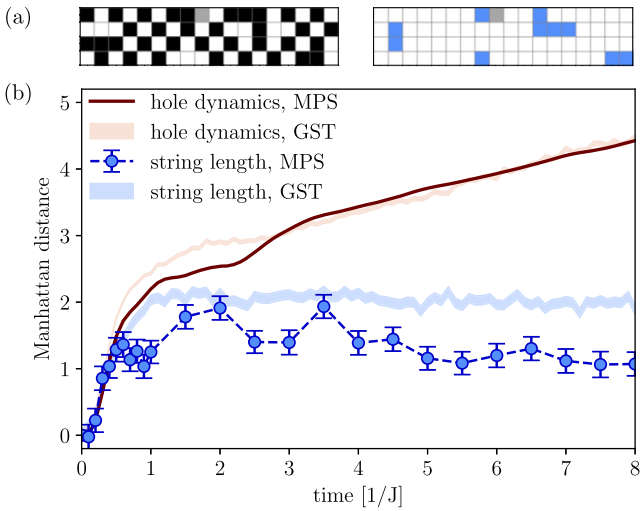

Figure 3. A parton interpretation of the hole dynamics for $t/J = 2$. (a) In the GST, spinon and chargon are bound together by a string of displaced spins. We extract string patterns by comparing to the perfect Néel state. In each snapshot, starting from the hole, the longest deviation from the Néel state without off-branches is taken as string pattern. (b) Average Manhattan distance of the hole to the origin and average string pattern length relative to time = 0 obtained from MPS snapshots are compared to GST predictions. The latter are obtained based on snapshots from the ground state of the Heisenberg model.

After the initial spreading out, which corresponds to the dynamics on the Bethe lattice, a further motion of the hole is restricted and the average Manhattan distance to the origin reaches a plateau. For longer times the dynamics of the spinon itself, introduced through spin-exchange processes on a time scale of $1/J$, becomes important. Within the GST, this corresponds to a motion of the origin of the Bethe lattice defined by the string states [37]. We thus observe a ballistically propagating hole, which corresponds to a heavily dressed magnetic polaron [38] with finite quasiparticle weight at zero temperature with a bandwidth proportional to J.

The quantum many-body state of the system is a superposition of many different Fock space configurations. When evaluating conventional observables such as the hole density, we thus average over a variety of string lengths and configurations. However, similar to measurements in a quantum gas microscope, we can numerically sample Fock space snapshots from the time evolved matrix product state (MPS). In each snapshot, we extract the string pattern as the longest connected deviation from the perfect Néel state originating from the hole [26, 34], see figure 3(a). Since the ground state of the t–J model itself already deviates from the Néel state, even at the starting point of the dynamics the average string pattern length is finite. We thus consider the difference of the average string pattern length to its value at time zero. The string pattern length grows at short times exactly as the distance of the hole to its initial point, see figure 3(b). As the velocity of the hole changes, the average string pattern length reaches a constant value, indicating the existence of a string which prevents a further separation of spinon and chargon.

In the following, we describe how one can quantitatively compare the analytic theory to the numerical data, see figure 3(b). Based on snapshots of the Heisenberg groundstate, we can use the predictions of the GST in combination with a simple theory for the spinon dynamics to generate a new dataset for each time step. Using a spinon dispersion extracted from reference [39], see also [37], we first sample the position of the spinon. We then place a hole at this site and move it through the system for a number of steps sampled from the string length distribution given by the GST, where in each step the direction is chosen randomly. From this new dataset, the distance of the hole to the center of the cylinder as well as the average length of the string pattern can be extracted as before. For both quantities, GST combined with spinon dynamics yields good agreement with the numerical simulations, see figure 3(b). At long times, the string pattern length extracted from the MPS snapshots decays slightly. We attribute this to interactions of the string with the spin environment, leading to an effective decay of the string length. In the GST, we do not take such effects into account, and thus the string pattern length stays constant after times $\propto 1/J$.

3. Infinite temperature

In quantum gas microscopy experiments, the temperature is always finite, with the lowest achieved values to date of $T/J = 0.5$ [21]. The results presented so far started from the ground state of the spin system, where long-range spin correlations are present. At finite temperature, the chargon dynamics should be well

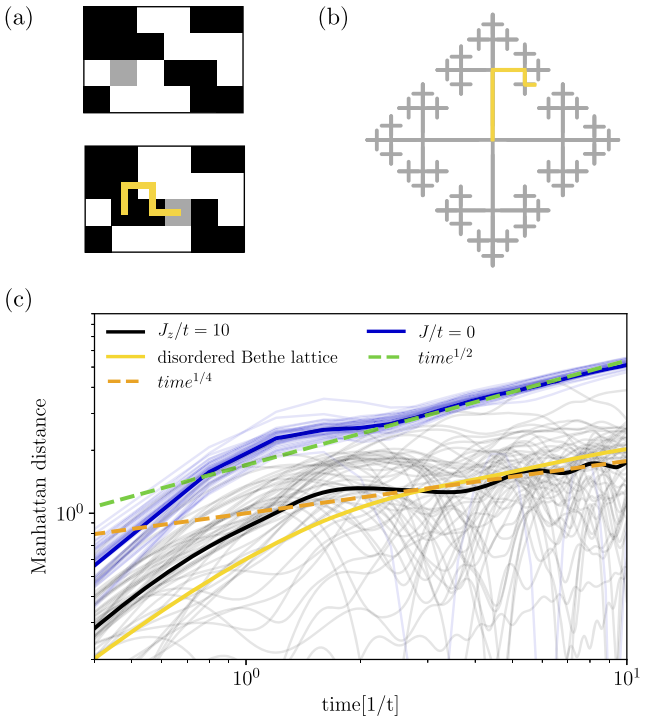

Figure 4. Dynamics of a hole in an infinite temperature initial state. (a) A hole is created in the center of a cylinder with a random configuration of spins. As the hole moves through the system, it rearranges the spins and thereby leaves a memory. (b) Its dynamics can therefore be approximated as a quantum random walk on the Bethe lattice. (c) For no spin couplings, $J = 0$, the hole spreads diffusively at intermediate times. In the case of strong Ising interactions, $J^z = 10t$, the spreading is limited to comparably short distances. The faint lines are the results for individual initial product states. Fluctuations strongly increase for finite J^z. The yellow line corresponds to the dynamics of a single particle on the Bethe lattice with a disorder potential.

described by the GST as long as the short range spin-correlations and thereby the string tension are finite. For current cold atom experiments [26, 38], we expect that our approach will accurately capture the formation of the magnetic polaron.

The opposite limit of infinite temperature can be studied by considering an ensemble of random product states. In this case, all spin correlations are zero and correspondingly the string tension vanishes. Nonetheless, the hole motion is associated with a memory effect in the spin system, since in general different paths taken by the hole lead to different spin configurations. Note that we still restrict the dynamics to the t–J model (1). In the case of $J \approx 0$, the hole dynamics can be approximated by a quantum random walk on the Bethe lattice [40], assuming that all paths are distinguishable and thus neglecting loops. Mapping back to the square lattice, this translates to diffusive behavior [16, 41]. For the spin 1/2-system considered here, different paths of the hole can lead to the same spin configuration. As a consequence, the diffusive behavior expected from the Bethe lattice calculation will be slightly modified [16]. As shown in figure 4, the average Manhattan distance of the hole to its initial point is consistent with diffusive behavior.

Introducing spin couplings effectively creates a disorder potential on the Bethe lattice. In order to simplify our theoretical picture, we here consider only Ising interactions. The disorder potential can be understood as follows: in each Fock space configuration, the motion of the hole by one site from i to j changes the energy of the spin system by $\Delta\epsilon_{\langle ij\rangle} = 0.25J^z\,(\Delta N_{\sigma\bar{\sigma}} - \Delta N_{\sigma\sigma})$, where $\Delta N_{\sigma(\bar{\sigma})\sigma}$ is the change in the number of (anti-)aligned spins on neighboring sites. The energy difference $\Delta\epsilon_{\langle ij\rangle}$ is therefore a random number between $\pm 0.5(\tilde{z}-1)J^z$ with $\tilde{z}$ the coordination number of the lattice. The hole motion can then be approximated by a quantum random walk on the Bethe lattice with a disorder potential $W_l = \sum_{\langle ij\rangle \in \Sigma} \Delta\epsilon_{\langle ij\rangle}$, where the sum runs over all bonds $\langle ij\rangle$ along the string Σ. For the spin configuration depicted in figure 4(a), the potential of the different hole position along the considered path is $W_l/J^z = 0, -1.5, 0, 0.5, 0.5$ for $l = 0, \ldots, 4$ for example. Note that for sites further apart on the Bethe lattice, the range of possible energy differences scales with the distance between the sites. In figure 4(b), we consider the case of strong Ising interactions, $J^z = 10t$, which could for example be realized with Rydberg interactions. Strong spin interactions lead to a strong disorder potential and thus the spreading of the hole is significantly reduced and consistent with subdiffusive spreading.

4. Summary and Outlook

In this work, we have studied the dynamics of a single hole created in a spin system. Our findings at zero temperature can be understood in the framework of a parton construction, where the original excitation is described by a chargon and a spinon connected by a string of displaced spins. For infinite temperature and no spin couplings, we confirm indications for diffusive behavior [15, 16] for longer times. This can be explained by the dynamics of a free particle on the Bethe lattice. Introducing Ising interactions adds a disorder potential, leading to hole dynamics consistent with subdiffusion in the limit of $J^z \gg t$.

In the future, it would be interesting to study the effect of finite temperature $0 < T < \infty$ on the observed behavior. For experimentally realistic temperatures of $T/J \approx 0.5$, the spin correlation functions, especially on short distances, are still sizable and thus the string tension is finite. The inverse temperature sets a timescale on which we expect a crossover from ballistic to diffusive behavior.

The case of infinite temperature and large Ising interactions is approximated by a particle moving on the Bethe lattice with a disordered potential, where the strength increases with the depth in the lattice. This scenario could be studied in more detail theoretically and possibly experimentally, for example with Rydberg interactions [33].

Starting from the ground state or low temperatures, the same analysis for the time evolution of the hole distance as well as the string pattern length could be applied in the case of adiabatically releasing the hole.

Another exciting direction for future research is the study of finite doping, especially the case of two holes. In the spirit of the analysis of single snapshots, it would be intriguing to see if string patterns connecting the two holes can be found or if they form two separate bound objects with a spinon each.

During review of our manuscript, the corresponding experiment has been performed in a quantum gas microscope and similar behavior at short and intermediate times as in figure 1 was found [42].

Acknowledgments

We would like to acknowledge fruitful discussions with Immanuel Bloch, Christie Chiu, Eugene Demler, Markus Greiner, Geoffrey Ji and Guillaume Salomon. We additionally want to thank Frank Pollmann and Ruben Verresen for providing important parts of the numerical code. We acknowledge support from the Technical University of Munich-Institute for Advanced Study, funded by the German Excellence Initiative and the European Union FP7 under Grant Agreement 291763, the Deutsche Forschungsgemeinschaft (DFG, German Research Foundation) under Germany's Excellence Strategy–EXC-2111–390814868, DFG Grant Nos. KN1254/1-1, DFG TRR80 (Project F8), from the European Research Council (ERC) under the European Union's Horizon 2020 research and innovation program (Grant Agreement No. 851161) and the Studienstiftung des deutschen Volkes.

References

[1] Lee P A, Nagaosa N and Wen X-G 2006 Doping a Mott insulator: physics of high-temperature superconductivity *Rev. Mod. Phys.* **78** 17–85
[2] Keimer B, Kivelson S A, Norman M R, Uchida S and Zaanen J 2015 From quantum matter to high-temperature superconductivity in copper oxides *Nature* **518** 179–86
[3] Auerbach A 1998 *Interacting Electrons and Quantum Magnetism* (Berlin: Springer)
[4] Dagotto E, Joynt R, Moreo A, Bacci S and Gagliano E 1990 Strongly correlated electronic systems with one hole: dynamical properties *Phys. Rev.* B **41** 9049–73
[5] Liu Z and Manousakis E 1992 Dynamical properties of a hole in a Heisenberg antiferromagnet *Phys. Rev.* B **45** 2425–37
[6] Leung P W and Gooding R J 1995 Dynamical properties of the single-hole t–J model on a 32-site square lattice *Phys. Rev.* B **52** R15711–4
[7] Brunner M, Assaad F F and Muramatsu A 2000 Single-hole dynamics in the t–J model on a square lattice *Phys. Rev.* B **62** 15480–92
[8] Mishchenko A S, Prokof'ev N V and Svistunov B V 2001 Single-hole spectral function and spin–charge separation in the t–j model *Phys. Rev.* B **64** 033101
[9] Golez D, Bonca J, Mierzejewski M and Vidmar L 2014 Mechanism of ultrafast relaxation of a photo-carrier in antiferromagnetic spin background *Phys. Rev.* B **89** 165118
[10] Jan K, Lenarcic Z, Golez D, Mierzejewski M, Peter P and Bonca J 2014 Multistage dynamics of the spin–lattice polaron formation *Phys. Rev.* B **90** 125104
[11] Zhang Q and Whaley K B 1991 Exact time-dependent propagation of vacancy motion in the t–J limit of the two-dimensional Hubbard Hamiltonian *Phys. Rev.* B **43** 11062–70
[12] Mierzejewski M, Vidmar L, Bonca J and Prelovcek P 2011 Nonequilibrium quantum dynamics of a charge carrier doped into a Mott insulator *Phys. Rev. Lett.* **106** 196401

[13] Lenarcic Z, Golez D, Bonca J and Prelovcek P 2014 Optical response of highly excited particles in a strongly correlated system *Phys. Rev.* B **89** 125123
[14] Eckstein M and Werner P 2014 Ultrafast separation of photodoped carriers in Mott antiferromagnets *Phys. Rev. Lett.* **113** 076405
[15] Carlström J, Prokof'ev N and Svistunov B 2016 Quantum walk in degenerate spin environments *Phys. Rev. Lett.* **116** 247202
[16] Kanász-Nagy M, Lovas I, Grusdt F, Greif D, Greiner M and Demler E A 2017 Quantum correlations at infinite temperature: the dynamical Nagaoka effect *Phys. Rev.* B **96** 014303
[17] Greif D, Uehlinger T, Jotzu G, Tarruell L and Esslinger T 2013 Short-range quantum magnetism of ultracold fermions in an optical lattice *Science* **340** 1307–10
[18] Hart R A *et al* 2015 Observation of antiferromagnetic correlations in the Hubbard model with ultracold atoms *Nature* **519** 211–4
[19] Parsons M F, Huber F, Mazurenko A, Chiu C S, Setiawan W, Wooley-Brown K, Blatt S and Greiner M 2015 Site-resolved imaging of Fermionic ^{6}Li in an optical lattice *Phys. Rev. Lett.* **114** 213002
[20] Cheuk L W *et al* 2016 Observation of spatial charge and spin correlations in the 2d Fermi–Hubbard model *Science* **353** 1260–4
[21] Mazurenko A *et al* 2017 A cold-atom Fermi–Hubbard antiferromagnet *Nature* **545** 462–6
[22] Hilker T A, Salomon G, Grusdt F, Omran A, Boll M, Demler E, Bloch I and Gross C 2017 Revealing hidden antiferromagnetic correlations in doped Hubbard chains via string correlators *Science* **357** 484–7
[23] Brown P T *et al* 2019 Bad metallic transport in a cold atom Fermi–Hubbard system *Science* **363** 379–82
[24] Nichols M A, Cheuk L W, Okan M, Hartke T R, Mendez E, Senthil T, Khatami E, Zhang H and Zwierlein M W 2019 Spin transport in a Mott insulator of ultracold Fermions *Science* **363** 383–7
[25] Salomon G, Koepsell J, Vijayan J, Hilker T A, Nespolo J, Pollet L, Bloch I and Gross C 2019 Direct observation of incommensurate magnetism in Hubbard chains *Nature* **565** 56–60
[26] Chiu C S, Ji G, Bohrdt A, Xu M, Knap M, Demler E, Grusdt F, Greiner M and Greif D 2019 String patterns in the doped Hubbard model *Science* **365** 251–6
[27] Vijayan J, Sompet P, Salomon G, Koepsell J, Hirthe S, Bohrdt A, Grusdt F, Bloch I and Gross C 2020 Time-resolved observation of spin–charge deconfinement in Fermionic Hubbard chains *Science* **367** 186–9
[28] Kjäll J A, Zaletel M P, Mong R S K, Bardarson J H and Pollmann F 2012 The phase diagram of the anisotropic spin-2 XXZ model: an infinite system DMRG study (arXiv:1212.6255)
[29] Zaletel M P, Mong R S K, Karrasch C, Moore J E and Pollmann F 2015 Time-evolving a matrix product state with long-ranged interactions *Phys. Rev.* B **91** 165112
[30] Gohlke M, Verresen R, Moessner R and Frank P 2017 Dynamics of the Kitaev–Heisenberg model *Phys. Rev. Lett.* **119** 157203
[31] Béran P, Poilblanc D and Laughlin R B 1996 Evidence for composite nature of quasiparticles in the 2d t–J model *Nucl. Phys.* B **473** 707–20
[32] Manousakis E 2007 String excitations of a hole in a quantum antiferromagnet and photoelectron spectroscopy *Phys. Rev.* B **75** 035106
[33] Grusdt F, Kánasz-Nagy M, Bohrdt A, Chiu C S, Ji G, Greiner M, Greif D and Demler E 2018 Parton theory of magnetic polarons: mesonic resonances and signatures in dynamics *Phys. Rev.* X **8** 011046
[34] Grusdt F, Bohrdt A and Demler E 2019 Microscopic spinon–chargon theory of magnetic polarons in the t–J model *Phys. Rev.* B **99** 224422
[35] Giamarchi T 2003 Quantum physics in one dimension *International Series of Monographs on Physics* (Oxford: Clarendon)
[36] Kruis H V, McCulloch I P, Nussinov Z and Zaanen J 2004 Geometry and the hidden order of Luttinger liquids: the universality of squeezed space *Phys. Rev.* B **70** 075109
[37] See supplementary online material (https://stacks.iop/NJP/22/123023/mmedia)
[38] Koepsell J, Vijayan J, Sompet P, Grusdt F, Hilker T A, Demler E, Salomon G, Bloch I and Gross C 2019 Imaging magnetic polarons in the doped Fermi–Hubbard model *Nature* **572** 358–62
[39] Martinez G and Horsch P 1991 Spin polarons in the t–J model *Phys. Rev.* B **44** 317–31
[40] Brinkman W F and Rice T M 1970 Single-particle excitations in magnetic insulators *Phys. Rev.* B **2** 1324–38
[41] Hart O, Yuan W and Castelnovo C 2020 Coherent propagation of quasiparticles in topological spin liquids at finite temperature *Phys. Rev.* B **101** 064428
[42] Ji G *et al* 2020 Dynamical interplay between a single hole and a Hubbard antiferromagnet (arXiv:2006.06672)
[43] Paeckel S, Köhler T, Swoboda A, Manmana S R, Schollwöck U and Hubig C 2019 Time-evolution methods for matrix-product states (arXiv:1901.05824)
[44] Hauschild J and Pollmann F 2018 Efficient numerical simulations with tensor networks: tensor network python (TeNPy) (arXiv:1805.00055)